Characterization of Interface Toughness in Thin-Ply Composites

Armanj D. Hasanyan,* and Sergio Pellegrino[†]

California Institute of Technology, Pasadena, CA, 91125, USA

Characterizing the interface bond of thin-ply composites is important for assessing the overall structural integrity. Due to the flexibility of thin composite laminates, it is not feasible to carry out mode I double cantilever beam (DCB) and mode II end notch flexure (ENF) tests, due to the large geometric changes undergone during testing. To reduce the compliance during testing, thick aluminum substrates are bonded to the two free-surfaces of the test laminates. DCB and ENF tests are specifically carried out in this configuration. A specific glass fiber plain weave interface of a 7-ply composite structure is tested. μCT imaging shows the presence of periodic voids of size scales of 200 μm, and local delaminated regions of $0.7 - 5.6$ mm. The former is attributed to capillary effects from the glass tows, while the latter is due to insufficient resin flow during the two-cure manufacturing process.

I. Introduction

Recent advances in tow-spreading technology [1], [2] have made it possible to manufacture composite laminates, with unidirectional prepregs of ply thicknesses as small as 17.5 μm, compared to conventional laminates, with ply thicknesses in the order of 190 μm. Experimental analysis of thin-ply laminates has shown improvements in the onset of damage (transverse cracking and delaminate), the ultimate strength, the fatigue and post-fatigue resistance, etc. [3]. This positive size effect is attributed to several factors, including a more homogeneous microstructure of the resulting composite compared to that of thicker plies.

Compliant 2 to 8-ply laminates using thin-plies are also currently being manufactured for applications requiring flexible composite structures. There is a growing interest for this in aerospace engineering, where lightweight, flexible composites are utilized in the areas of origami structures [4], morphing wings [5], energy harvesting [6], etc. For space applications, thin-ply laminates are currently being used for deployable booms and longerons for solar arrays and antenna. The thin-ply composite structures are ideal for achieving high packaging efficiency for space structure applications. The packaging is usually achieved by tightly coiling composite booms (or longerons) around a rigid mandrel. These structures were included in the demonstration of the Roll-Out Solar Array (ROSA) on the International Space Station [7]. Thin-ply composites were also used as part of the 2003 Mars Advanced Radar for Subsurface and Ionospheric Sounding (MARSIS) antenna [8]. Coilable thin-ply composites are also currently being developed for the space-based solar power (SSP) project at Caltech [9], [10], for deploying a structure with integrated photovoltaic cells and RF power transfer capability. In the SSP structure, thin-ply composites are used in a double tape spring configuration, similar to the Triangular Rollable And Collapsible (TRAC) longeron design [11], [12]. The main components of the longeron cross section are the flanges, made out of thin-ply composites, bonded at the web section during manufacturing. The main geometric parameters are the radius of curvature of the flanges r, thickness t, opening angle θ, and width of the web w. For stowage and deployment, the flanges are flattened, and the structure is coiled around a rigid cylindrical hub of radius R. During the manufacturing of the TRAC longeron, the structure is cured in two-stages. First, the plies in the flanges are bonded through curing, and then the flanges are joined together at the web for bonding during a second curing process. Due to the second cure process, the flanges are not perfectly bonded, and have the potential to debond at the web. For this, the characterization of the interface bond is necessary.

The failure analysis of thin-ply composites at the constitutive level is still unexplored. The main challenge is due to the compliance of the laminates, which limit the applicability of conventional testing approaches for thicker ply composites. To address this, a testing approach is considered for determining the interface delamination strength of thin-ply composite structures. Although this approach is applicable to thin-ply composites in general, here it is applied

---

*Postdoctoral Researcher, Graduate Aerospace Laboratories, 1200 E California Blvd. MC 105-50, Pasadena, CA. AIAA Member. e-mail: armanj@caltech.edu

[†]Joyce and Kent Kresa Professor of Aerospace and Civil Engineering, Graduate Aerospace Laboratories, 1200 E California Blvd. MC 105-50, Pasadena, CA. AIAA Fellow. e-mail: sergiop@caltech.edu

to characterize the interface bond of the web-section of the coilable longeron shown in Fig. 1. This study addresses the potential delamination of the web leading to the longeron loosing its overall structural integrity. This is especially important, since X-ray microtomography, or μCT imaging of the web showed the presence of significant manufactured induced voids, which will be discussed in section III.
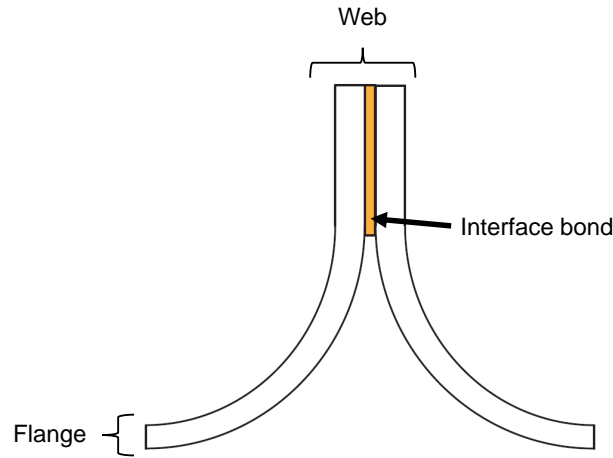
Fig. 1   Cross-section of coilable longeron for SSP structure.

II. Mode I and Mode II Strain Energy Release Rates

Delamination is one of the primary failure modes in composites. Even though thin-ply composites are in general resistant to inner-ply delamination, they can be expected to occur in bonded regions, such as in the web of the cross-section in Fig. 1. In the literature, many different testing methods have been developed for this purpose. The two most widely used test configurations are the classical double cantilever beam (DCB) and the end notch flexure (ENF) tests for mode I and mode II interface strengths, respectively. In conducting these tests, the interface strength of the bond is characterized through the critical mode I and mode II strain energy release rates.

The experimental configuration for obtaining the critical mode I interlaminar fracture toughness G_I^C according to ASTM D5528 [13] is shown in Fig. 2. The test is conducted on a N-ply laminate of uniform thickness t with in-plane dimensions of length L and width b. In preparing this structure, an initial crack of length a is introduced at the mid-plane, usually in the manufacturing phase, through a nonadhesive insert. For mode I testing, piano hinges (or loading blocks) are bonded at the ends in order to apply tension to induce mode I loading.
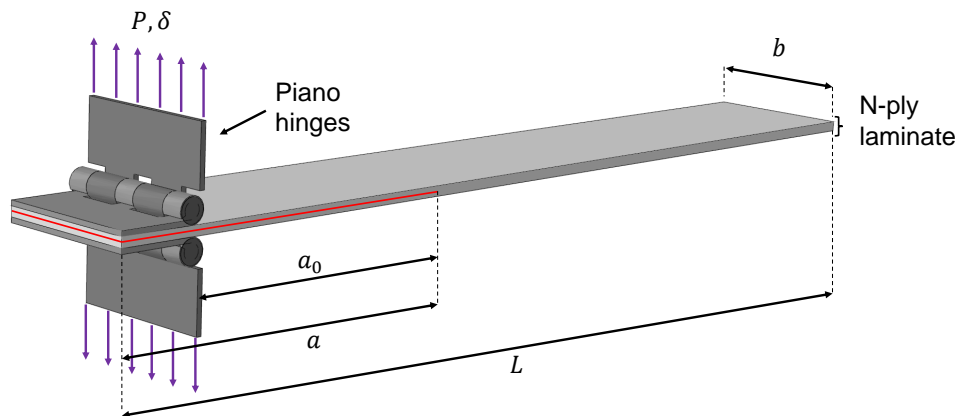
Fig. 2   Double cantilever beam (DCB) mode I testing setup.

In general, the critical strain energy release rate G^C is defined on the basis of linear elastic fracture mechanics

(LEFM) as

$$G^C = \frac{P_C^2}{2b}\frac{\partial C}{\partial a} = \frac{P_C\delta_C}{2bC}\frac{\partial C}{\partial a} \tag{1}$$

where P_C and δ_C are the critical load and displacement, respectively, at which the crack propagates, b is the width of the specimen, C is the compliance, and a is the crack length. Assuming clamped boundary conditions at the delamination, the relation between compliance of the structure and crack length from Eqn. 1 results in [13]

$$G_I^C = \frac{3P_C\delta_C}{2ba} \tag{2}$$

The value of G_I^C defined from Eqn. 2 is only valid for the assumed boundary conditions. To take into account the rotation and deflection at the crack-tip, large displacements present in the specimen, and stiffening due to the presence of the piano hinges, G_I^C can be evaluated from the Modified Beam Theory (MBT), where the crack length a_0 is increased with a correction term Δ. As a result, the value of G_I^C is evaluated using the formula

$$G_I^C = \frac{3P_C\delta_C}{2b(a_0 + |\Delta|)} \tag{3}$$

Because the compliance C is proportional to $(a + |\Delta|)^3$, the correction term $|\Delta|$ is determined by plotting $C^{1/3}$ against the crack length a, from which the correction term is found as the intercept of the extrapolation of the experimental values to $C^{1/3} = 0$. Further details on the MBT method can be found in [13].

Similarly, the critical mode II interlaminar fracture toughness G_{II}^C is evaluated through the ENF test shown in Fig. 3. The test configuration is a 3-point bending experiment, performed on a notched sample, of length a_0, and a total length of L. After obtaining the relation between the compliance of the structure and crack length, the mode II strain energy release rate G_{II}^C can be calculated according to Eqn. 1, which results in

$$G_{II}^C = \frac{9P_C\delta_C a^2}{2b(2L^3 + 3a_0^3)} \tag{4}$$

where P_C and δ_C are evaluated at the critical point at which the crack propagates.
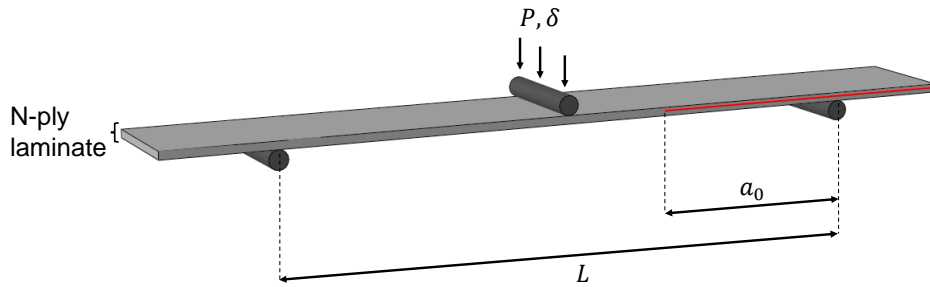
Fig. 3   End notch flexure (ENF) mode II testing setup.

A. Stiffening of thin-ply laminates for DCB and ENF testing

It should be noted that the DCB and ENF tests described above, the evaluation of the strain energy release rates G_I^C and G_{II}^C are predicated on the assumption of linear elastic fracture mechanics (LEFM), with the laminate deforming in the geometrically linear regime. Because of this restriction, direct testing of thin-ply laminate structures to characterize the interface strength is not possible because of the high compliance of the test samples. Because the values of G_I^C and G_{II}^C are considered as material properties, which are therefore independent of the thickness of the laminate, their values can be measured by conducting the DCB and ENF tests on a stiffened laminate structure. Therefore, two additional substrate layers are bonded to the top and bottom surfaces of the original laminate, as shown in Fig. 4.

3
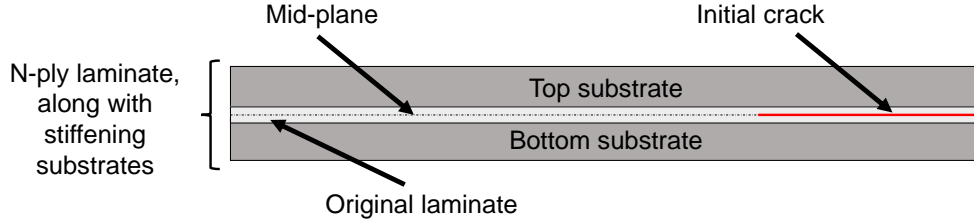
Fig. 4 Schematic (not drawn to scale) of the bonded substrates to stiffen the flexible laminate structure.

Note that, although the bonding of additional substrate layers is considered here for the first time for suppressing large geometric deformations of thin-ply composites, this approach has been used before in the DCB and ENF tests. Examples include the suppression of premature bending failures in the DCB and ENF experiments, to ensure delamination growth during tests [14]. In addition, in [15] and [16], for interface testing of fiber-metal laminates (GLARE), aluminum layers were bonded on the top and bottom surfaces of the sample in order to suppress material nonlinearity (plasticity) from the metal plies when conducting DCB and ENF tests.

III. Manufacturing of Thin-Ply Laminates

The laminate system considered in this study is the web-section of the SSP TRAC longeron structure. The manufacturing process and the composite system is discussed in [11], [12]. The flanges are made of thin-plies of plain weave glass fiber fabric (GFPW) and unidirectional carbon fiber (UDCF) tapes. The GFPW is a prepreg made of JPS E-glass fabric (style 1067) and Patz PMT-F4 epoxy resin, while the UDCF is Torayca T800 carbon fibers with NTPT ThinPreg 402 epoxy resin. The ply thicknesses of the GFPW and UDCF are 25 μm and 35.5 μm, respectively. The flanges of the longeron are composed of 3-plies of $[\pm45_{GFPW}/0_{UDCF}/\pm45_{GFPW}]$. This type of laminate is known as FlexLam, which was developed by the Air Force Research Laboratory (AFRL) [17]. During manufacturing, two sets of 3-plies are separately placed over 1.6 m long, U-shaped aluminum molds for the first cure process. Next, a single layer of GFPW is sandwiched between the 3-ply flanges at the web-section for a second cure. The stacking of the resulting 7-ply laminate structure is $[\pm45_{GFPW}/0_{UDCF}/\pm45_{GFPW}/\pm45_{GFPW}/\pm45_{GFPW}/0_{UDCF}/\pm45_{GFPW}]$. It has been determined that the additional GFPW ply at the interface of the web bond provides a stronger bond. However, it is important to better understand and characterize the bonding of the two flanges at the web-section.

For the samples considered in this study, only the 7-ply laminate was manufactured using the 2-cure process, without the cured 3-ply flanges, which have no effect on the interface bond. The resulting manufactured structure was 1.6 m long, as shown in Fig. 5.

To better understand the bonding of the interface, micro computed tomography (μCT) imaging of the web was performed. In Fig. 6, the middle GFPW ply is shown. From the images of the plain weave structure, periodic micro-voids were observed throughout the interface. The size of the voids is approximately 200 μm. Due to the periodic nature of these voids, their location at the edge tow, these these defects are attributed to capillary effects, which produce unsaturated zones of matrix voids. Fig. 7 shows 8 images with a larger field of view taken along the manufactured web. At this scale, large delaminated areas are observed at the interface, with lengths of $0.7 - 5.6$ mm. These large voids are attributed to insufficient resin flow. As a summary, two scales of manufacturing defects were found at the web interface. As a result, characterizing the interface strength of this imperfect bonded region is crucial.

IV. Preparation of Samples for DCB and ENF Testing

The 7-ply laminates were prepared for the DCB and ENF tests. The steps for preparing the samples are shown in Fig. 8. (a)The 1.6 m long laminate was cut into 200 mm long individual pieces, by using a standard box cutter. (b) An initial crack of length $a_0 = 70$ mm was introduced. Because the bonding at the web interface is not perfect, it was easy to separate the two sides using a box cutter, after which they were carefully peeled until a crack of size $a_0 = 70$ mm had been reached. In this way, eight 200 mm long samples were obtained from a single web.
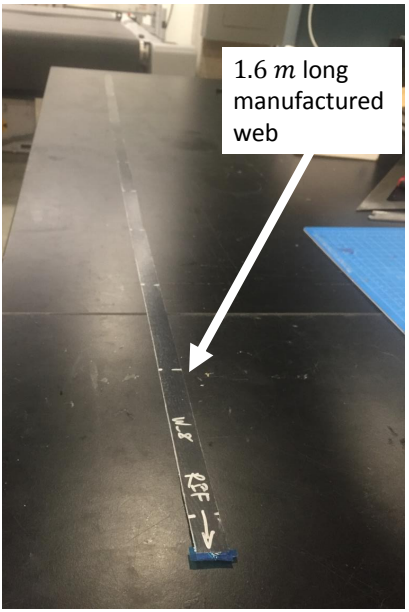
Fig. 5   7-ply composite web used for DCB and ENF tests.
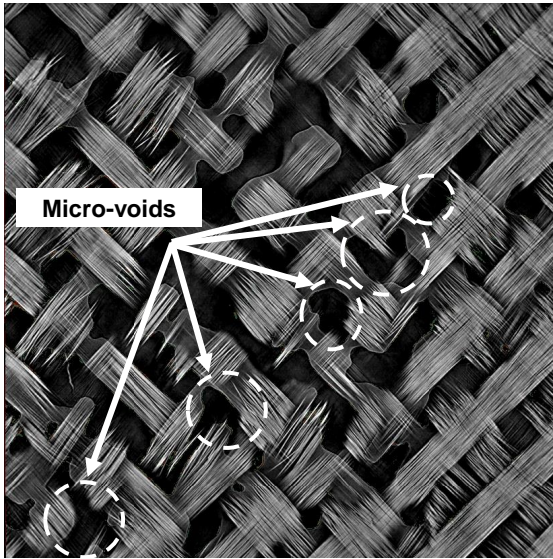
Fig. 6   Micro-voids observed in the GFPW-GFPW interface.

(a)

(b)

(c)

(d)

(e)

(f)

(g)

(h)
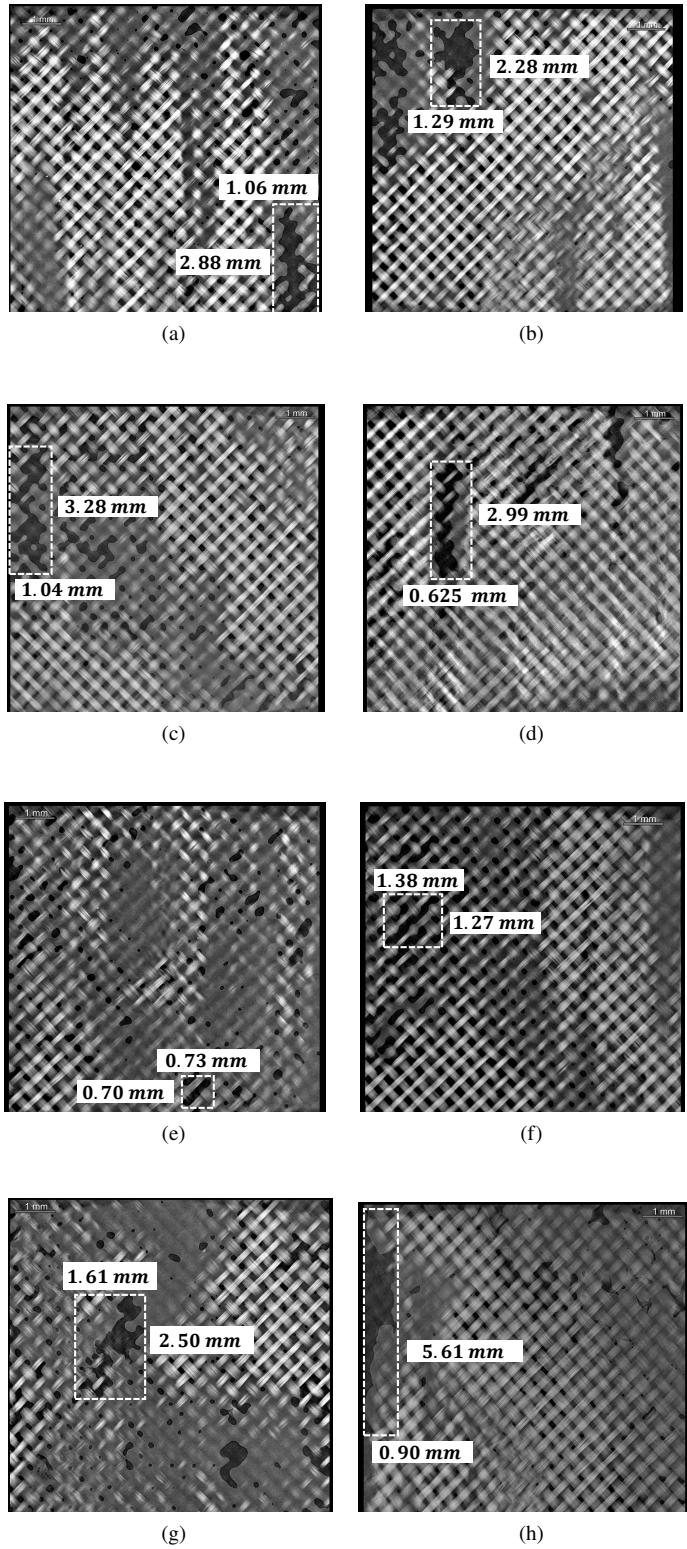
Fig. 7   Voids and delaminations due to insufficient resin flow during manufacturing.
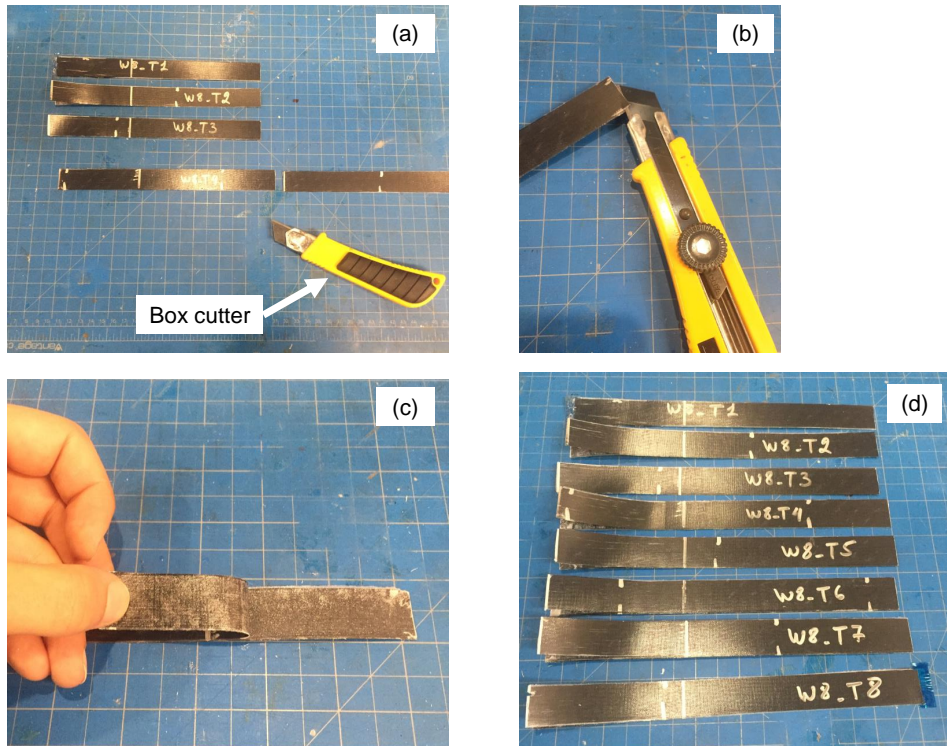
Fig. 8   Preparation of the web for DCB and ENF testing.

Once the initial crack a_0 had been introduced, two aluminum (Al 7075) substrates, each with a thickness of 1.6 m were bonded to the top and bottom surfaces of the flexible composite. The aluminum substrates had the dimensions of 8×200 mm. They were cut from a 300×600 mm plate using a waterjet cutter. To bond the aluminum substrates to the web, Loctite EA E-60HP adhesive was used. At the crack opening, nonadhesive teflon inserts were used to prevent the adhesive from flowing into the crack surfaces during bonding. Clamps were placed throughout the length of the sample in order to ensure sufficient pressure was applied during bonding, as shown in Fig. 9. After 24 hours, the clamps were removed and the sides of the sample were cleaned using a box cutter to remove any additional adhesive which had flowed out. In addition, piano hinges were bonded to the ends of the DCB samples following the same procedure. In concluding the tests, three 1.6 m long, 7-ply laminates were manufactured for mode I testing. Similarly, four 1.6 m long laminates were made for mode II.

V. Experimental Results

After the samples had been prepared, mode I and mode II tests were conducted using an Instron machine. The placement of the samples for the two types of tests is shown in Fig. 10.

For mode I, the piano hinges were gripped with the Instron. Tension load was applied in order to separate the initially debonded surfaces to induce a mode I load. For mode I tests, red marks were placed on the test samples, with spacing of 5 mm in order to track the growth of the crack length with the applied load. The growth of the crack was tracked using a video camera, which was placed perpendicular to the sample. For mode I, the loading rate was 2.0 mm/min, on a load cell with a capacity of 1000 N. From this data, the plot of the cube root of the compliance vs crack size a was plotted for each sample, from which, the MMB correction term Δ was determined. The mode I strain energy release rate G_I^C was then evaluated using Eqn. 3, where the peak load and displacement was taken from the force-displacement recordings of the Instron machine, as shown in Fig. 10a.

The ENF test procedure was similar (Fig. 10b). The test sample was placed on a 3-point bending fixture for testing. The contact loading point was moved vertically down, while the two end supports were held in place. The load was applied at a rate of 0.5 mm/min, on a load cell with a capacity of 1000 N. From the resulting load-displacement
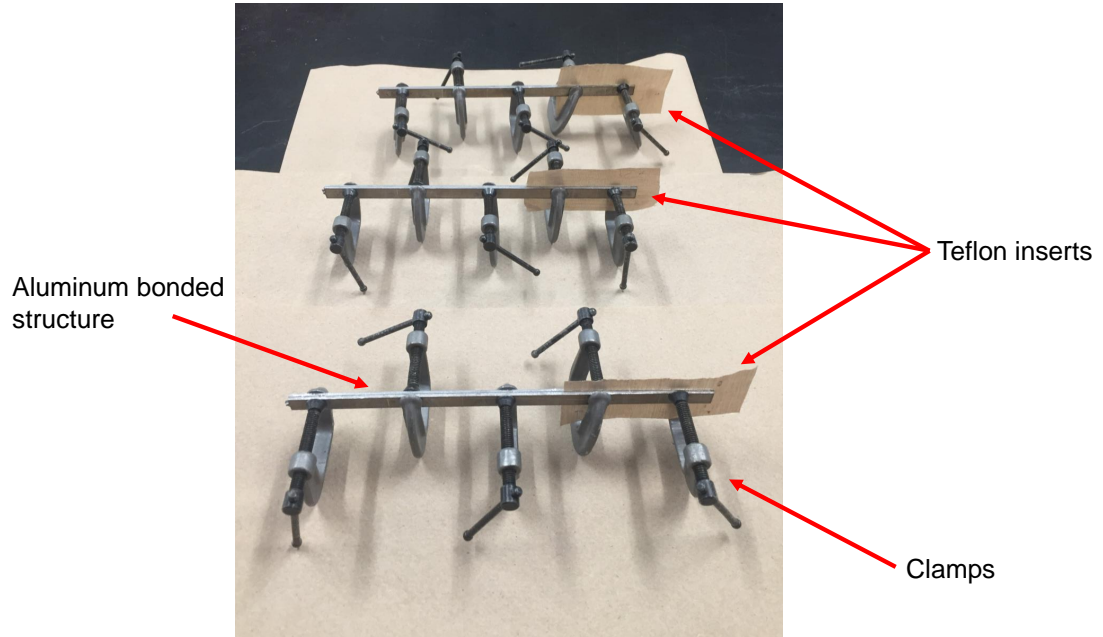
Fig. 9 Bonding of Al substrates to the flexible laminate.

recording, the critical mode II strain energy release rate G_{II}^C was calculated using Eqn. 4.

Of the 24 samples, 10 were debonded was due to premature debonding of the aluminum substrate from the composite during testing. This was observed both visually and it was recorded on the load-displacement curve. The results for the remaining samples for mode I tests in Fig. 11 show the calculated value of G_I^C vs position along the web section. The variability of these results is attributed to the porosity of the interface, shown in Fig. 6 and Fig. 7. For the mode I tests, the mean value of G_I^C was $G_I^{C,avg} = 0.315 \ kJ/m^2$, with a standard deviation $G_I^{C,std} = 0.07 \ kJ/m^2$.

In the mode II test, 22 out of 32 samples resulted in delamination at the web interface. The results of the 22 sample tests are plotted in Fig. 12. Values of G_{II}^C have a mean of $G_{II}^{C,avg} = 0.616 \ kJ/m^2$, and a standard deviation of $G_{II}^{C,std} = 0.139 \ kJ/m^2$.

VI. Conclusion

In this work, a simple method for characterizing the interface of flexible thin-ply laminates was introduced. To suppress the flexibility of the structure, aluminum substrates were bonded on the top and bottom surfaces of the composite. This was to reduce the overall compliance of the flexible structure. With the stiffened structure, mode I DCB and mode II ENF tests were done to characterize the interface of the laminate. The resulting values of G_I^C and G_{II}^C showed that the values were stochastic, with the mean and standard deviation of mode I being $G_I^{C,avg} = 0.315 \ kJ/m^2$ and $G_I^{C,std} = 0.07 \ kJ/m^2$, respectively, and for mode II, $G_{II}^{C,avg} = 0.616 \ kJ/m^2$ and $G_{II}^{C,std} = 0.139 \ kJ/m^2$. This is attributed to the high porosity of the interface, which is induced by capillary effects of bonding 2-plies of GFPW, and due to insufficient resin flow, which was shown in Fig. 6 and Fig. 7. The tests were conducted to evaluate the interface bond strength of the SSP longeron web-section, however, the method of adding substrates to flexible laminates can be further generalized for testing other thin-ply interfaces.

References

[1] Sihn, S., Kim, R. Y., Kawabe, K., and Tsai, S. W., "Experimental studies of thin-ply laminated composites," *Composites Science and Technology*, Vol. 67, No. 6, 2007, pp. 996–1008.

(a)

(b)
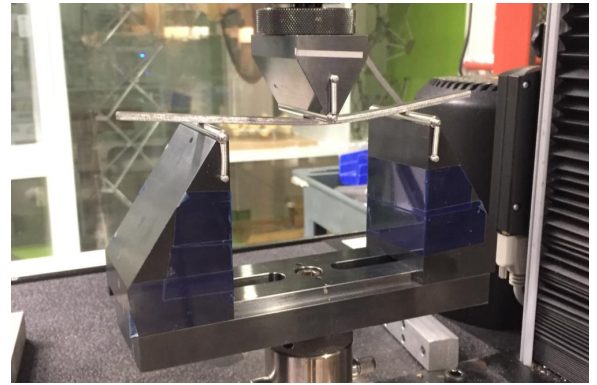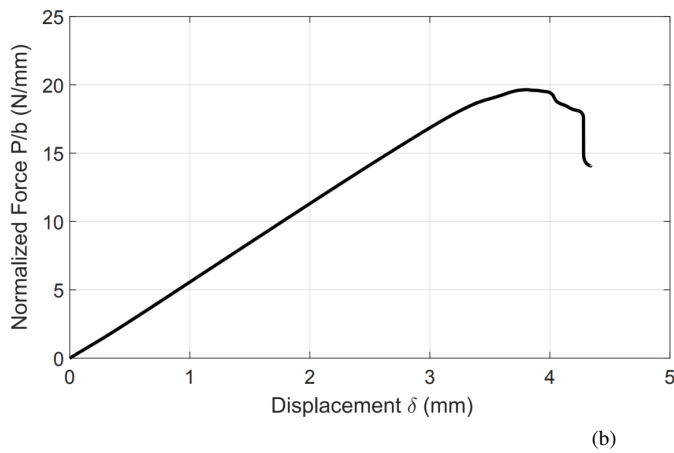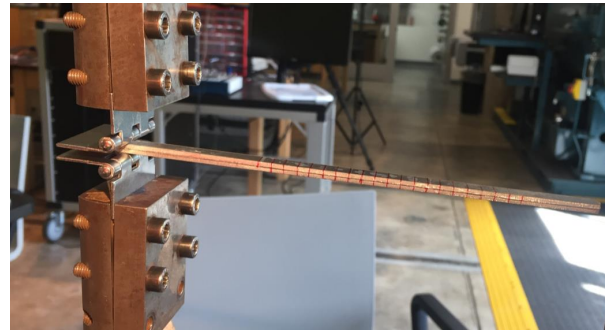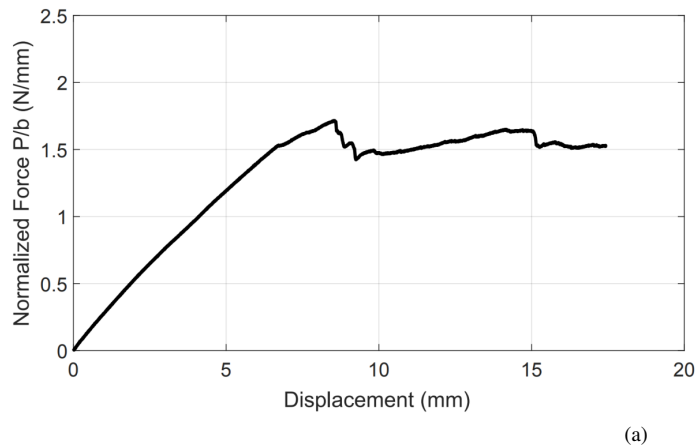
Fig. 10   Experimental setup on Instron machine for a) mode I DCB and b) mode II ENF testing and the corresponding force-displacement recording.
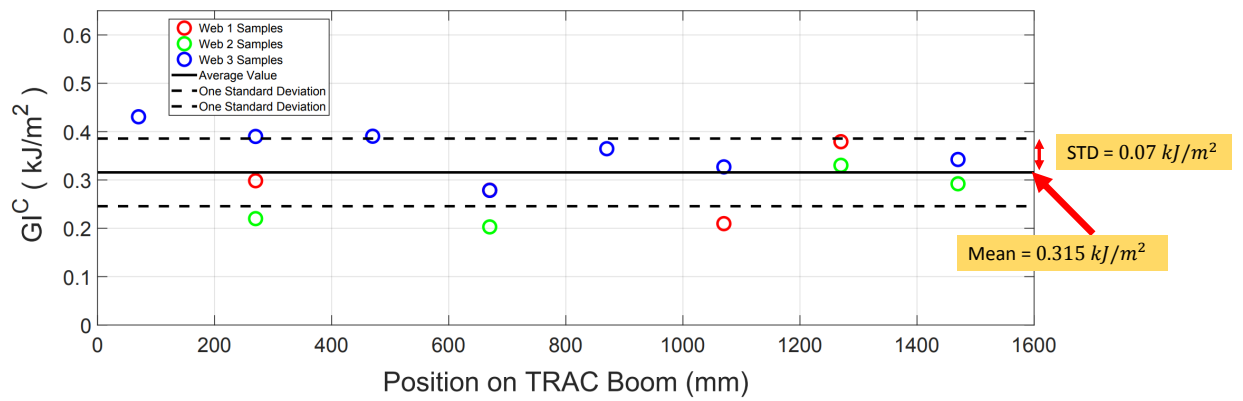
Fig. 11   Measured values of G_I^C vs position along the manufactured web.
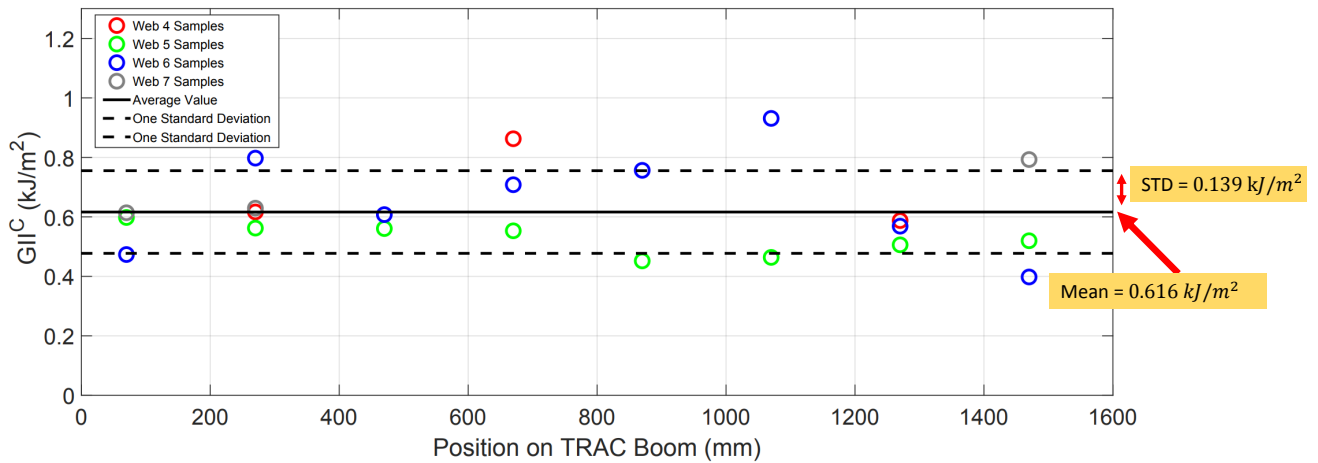
Fig. 12   Measured values of G_{II}^C vs position along the manufactured web.

[2]   El-Dessouky, H. M., "6 Spread Tow Technology for Ultra Lightweight CFRP Composites: Potential and Possibilities," *Advanced Composite Materials: Properties and Applications*, Sciendo Migration, 2017, pp. 323–348.

[3]   Amacher, R., Cugnoni, J., and Botsis, J., "Thin ply composites: experimental characterization and modeling," *19th International Conference on Composite Materials*, 2013.

[4]   Cozmei, M., Hasseler, T., Kinyon, E., Wallace, R., Deleo, A. A., and Salviato, M., "Aerogami: Composite Origami Structures as Active Aerodynamic Control," *arXiv preprint arXiv:1909.04119*, 2019.

[5]   Kota, S., Osborn, R., Ervin, G., Maric, D., Flick, P., and Paul, D., "Mission adaptive compliant wing–design, fabrication and flight test," *RTO Applied Vehicle Technology Panel (AVT) Symposium*, RTO-MP-AVT-168, Evora, Portugal, 2009.

[6]   Lee, A. J., and Inman, D. J., "A multifunctional bistable laminate: snap-through morphing enabled by broadband energy harvesting," *Journal of Intelligent Material Systems and Structures*, Vol. 29, No. 11, 2018, pp. 2528–2543.

[7]   Banik, J., Kiefer, S., LaPointe, M., and LaCorte, P., "On-orbit validation of the roll-out solar array," *2018 IEEE Aerospace Conference*, IEEE, 2018, pp. 1–9.

[8]   Mobrem, M., and Adams, D., "Deployment analysis of the lenticular jointed antennas onboard the mars express spacecraft," *Journal of Spacecraft and Rockets*, Vol. 46, No. 2, 2009, pp. 394–402.

[9]   Gdoutos, E., Leclerc, C., Royer, F., Kelzenberg, M. D., Warmann, E. C., Espinet-Gonzalez, P., Vaidya, N., Bohn, F., Abiri, B., Hashemi, M. R., et al., "A lightweight tile structure integrating photovoltaic conversion and RF power transfer for space solar power applications," *2018 AIAA Spacecraft Structures Conference*, 2018, p. 2202.

[10] Gdoutos, E., Leclerc, C., Royer, F., Türk, D. A., and Pellegrino, S., "Ultralight spacecraft structure prototype," *AIAA Scitech 2019 Forum*, 2019, p. 1749.

[11] Leclerc, C., Pedivellano, A., and Pellegrino, S., "Stress Concentration and Material Failure During Coiling of Ultra-Thin TRAC Booms," *2018 AIAA Spacecraft Structures Conference*, 2018, pp. 1–16.

[12] Leclerc, C., and Pellegrino, S., "Reducing Stress Concentration in the Transition Region of Coilable Ultra-Thin-Shell Booms," *AIAA Scitech 2019 Forum*, 2019, pp. 1–15.

[13] AC09036782, A., *Standard test method for mode I interlaminar fracture toughness of unidirectional fiber-reinforced polymer matrix composites*, ASTM Internat., 2007.

[14] Reeder, J. R., Demarco, K., and Whitley, K. S., "The use of doubler reinforcement in delamination toughness testing," *Composites Part A: Applied Science and Manufacturing*, Vol. 35, No. 11, 2004, pp. 1337–1344.

[15] Lopes, C. S., Remmers, J. J., and Gürdal, Z., "Influence of porosity on the interlaminar shear strength of fibre-metal laminates," *Key Engineering Materials*, Vol. 383, Trans Tech Publ, 2008, pp. 35–52.

[16] Airoldi, A., Vesco, M., Van Der Zwaag, S., Baldi, A., Sala, G., et al., "Damage in GLARE laminates under indentation loads: experimental and numerical results," *Proceedings of the 17th international conference on composite materials*, 2009.

[17] Pollard, E., and Murphey, T., "Development of deployable elastic composite shape memory alloy reinforced (DECSMAR) structures," *47th AIAA/ASME/ASCE/AHS/ASC Structures, Structural Dynamics, and Materials Conference 14th AIAA/ASME/AHS Adaptive Structures Conference 7th*, 2006, p. 1681.